Centrality Dependence of Charged-Particle Pseudorapidity Distributions from d + Au Collisions at $\sqrt{s_{NN}} = 200 \, \text{GeV}$

I. Arsene,[10] I. G. Bearden,[7] D. Beavis,[1] C. Besliu,[10] B. Budick,[6] H. Bøggild,[7] C. Chasman,[1] C. H. Christensen,[7]
P. Christiansen,[7] J. Cibor,[3] R. Debbe,[1] E. Enger,[12] J. J. Gaardhøje,[7] M. Germinario,[7] K. Hagel,[8] H. Ito,[1,11] A. Jipa,[10]
J. I. Jørdre,[9] F. Jundt,[2] C. E. Jørgensen,[7] R. Karabowicz,[4] E. J. Kim,[1,11] T. Kozik,[4] T. M. Larsen,[12] J. H. Lee,[1] Y. K. Lee,[5]
S. Lindal,[12] R. Lystad,[9] G. Løvhøiden,[12] Z. Majka,[4] A. Makeev,[8] M. Mikelsen,[12] M. Murray,[8,11] J. Natowitz,[8]
B. Neumann,[11] B. S. Nielsen,[7] D. Ouerdane,[7] R. Płaneta,[4] F. Rami,[2] C. Ristea,[10] O. Ristea,[10] D. Röhrich,[9] B. H. Samset,[12]
D. Sandberg,[7] S. J. Sanders,[11] R. A. Sheetz,[1] P. Staszel,[4,7] T. S. Tveter,[12] F. Videbæk,[1] R. Wada,[8] Z. Yin,[9] and I. S. Zgura[10]

(BRAHMS Collaboration)

[1]*Brookhaven National Laboratory, Upton, New York 11973, USA*
[2]*Institut de Recherches Subatomiques and Université Louis Pasteur, Strasbourg, France*
[3]*Institute of Nuclear Physics, Krakow, Poland*
[4]*Jagiellonian University, Krakow, Poland*
[5]*Johns Hopkins University, Baltimore, Maryland 21218, USA*
[6]*New York University, New York, New York 10003, USA*
[7]*Niels Bohr Institute, University of Copenhagen, Copenhagen 2100, Denmark*
[8]*Texas A&M University, College Station, Texas 77843, USA*
[9]*Department of Physics, University of Bergen, Bergen, Norway*
[10]*University of Bucharest, Bucharest, Romania*
[11]*University of Kansas, Lawrence, Kansas 66045, USA*
[12]*Department of Physics, University of Oslo, Oslo, Norway*

Charged-particle pseudorapidity densities are presented for the d + Au reaction at $\sqrt{s_{NN}} = 200 \, \text{GeV}$ with $-4.2 \leq \eta \leq 4.2$. The results, from the BRAHMS experiment at BNL Relativistic Heavy-Ion Collider, are shown for minimum-bias events and 0%–30%, 30%–60%, and 60%–80% centrality classes. Models incorporating both soft physics and hard, perturbative QCD-based scattering physics agree well with the experimental results. The data do not support predictions based on strong-coupling, semiclassical QCD. In the deuteron-fragmentation region the central 200 GeV data show behavior similar to full-overlap d + Au results at $\sqrt{s_{NN}} = 19.4 \, \text{GeV}$.

The saturation of initial parton densities in relativistic heavy-ion collisions, a manifestation of high-density QCD, is expected to significantly influence the pseudorapidity and centrality dependence of the emitted charged-particle densities from these reactions [1–5]. Earlier charged-particle pseudorapidity-density distributions for Au + Au collisions [6–11] from the BNL Relativistic Heavy-Ion Collider (RHIC) have been used to constrain model predictions for ultrarelativistic heavy-ion collisions. They have been inconclusive, however, as to whether parton saturation in the initial-state contributes significantly to the reaction dynamics, with both the saturation model [3,4] and calculations that instead focus on the energy-loss mechanisms for the multiple minijets created in the collisions [12–15] successfully describing the data. A similar model ambiguity found in explaining the observed suppression of high-p_t particles in Au + Au collisions was recently resolved with midrapidity d + Au data showing the suppression is not an initial-state effect [16–19]. It has been suggested [5] that global particle yields in d + Au

collisions might result in a definitive signature of parton saturation.

We report on a measurement of the charged-particle pseudorapidity densities for the d + Au reaction at $\sqrt{s_{NN}} = 200 \, \text{GeV}$ with pseudorapidity η coverage of $-4.2 \leq \eta \leq 4.2$. The pseudorapidity densities are reported for minimum-bias events and 0%–30%, 30%–60%, and 60%–80% centrality classes. The results allow for a detailed comparison to model predictions of particle production at RHIC energies. The most central data (0%–30%), where both deuteron nucleons are expected to participate in the reaction, are compared with full-overlap d + Au data obtained by the NA35 collaboration at $\sqrt{s_{NN}} = 19.4 \, \text{GeV}$ [20].

The present analysis employs several of the BRAHMS global detector subsystems: The Si multiplicity array (SiMA) and the scintillator tile multiplicity array (TMA) [21] are used for centrality determination and to measure the pseudorapidity densities close to midrapidity. The beam-beam counter (BBC) arrays are used to reconstruct

the collision vertex and to determine the pseudorapidity densities at larger pseudorapidities. The "inelasticity counters" (INEL), developed for the $pp2pp$ experiment [22], are used for a close-to-minimum-bias experiment trigger and to provide vertex position information in cases where the beam-beam counter arrays are not able to establish this information. Full details of the BRAHMS apparatus can be found in Ref. [23].

The layout of the SiMA and TMA detectors for the $d +$ Au experiment is similar to that presented for earlier measurements of Au + Au multiplicities at $\sqrt{s_{NN}} =$ 130 GeV and 200 GeV, and details of the analysis procedures can be found in Refs. [9,10]. The SiMA was configured with 25, 4 cm × 6 cm Si wafers in a hexagonal arrangement around the beam pipe, with each wafer functionally divided into seven discrete segments along the beam line and located 5.3 cm from the beam axis. Four sides of the hexagonal array were populated with six detectors, each, with the remaining two sides left largely unpopulated except for a single wafer mounted outside the acceptance of either of the BRAHMS spectrometers [23]. The TMA was populated with 38, 12 cm × 12 cm plastic scintillator tiles with fiber-optic readout located 13.7 cm from the beam axis. The hexagonal TMA array had four sides fully populated with eight detectors, each, with two and four detectors mounted on the other two sides, respectively. With this arrangement, the SiMA and TMA can each cover the pseudorapidity range $-2.2 \leq \eta \leq 2.2$ for collisions at array center. In the analysis, a range of collision vertex locations z about the nominal array center is used, with $-15 \text{ cm} \leq z \leq 15 \text{ cm}$. Particle multiplicities were deduced for an individual SiMA and TMA element by using GEANT [24] simulations to convert the observed energy-loss signal to the number of primary particles hitting that element. The HIJING event simulator [12] was used to obtain the initial distribution of particle types and momenta.

Two beam-beam counter arrays, positioned around the beam pipe on either side of the nominal interaction point at a distance of 2.20 m, are used to extend coverage out to $\eta = \pm 4.2$. Each array consists of separate sets of small (19 mm diameter) and large (51 mm diameter) Cherenkov UV-transmitting plastic radiators coupled to photomultiplier tubes. Leading particle timing achieves a vertex position resolution of ≈ 2 cm. Charged-particle multiplicities are deduced from the number of particles hitting each detector, as found by dividing the measured analog-to-digital converter signal by that corresponding to a single incident particle.

Three pairs of INEL counters were used to develop a near-to-minimum-bias trigger by detecting charged particles in the pseudorapidity range $3.2 < |\eta| < 5.3$. The basic INEL counter consists of a plastic scintillator ring that is segmented into four pieces and arranged about the beam pipe. The counter locations with respect to the nominal

vertex and (inner radius; outer radius) were ±155 cm (4.13 cm; 12.7 cm), ±416 cm (6.67 cm; 12.7 cm) and ±660 cm(6.67 cm; 12.7 cm). Relative time-of-flight measurements with the INEL arrays lead to an interaction vertex determination with a resolution of ≈ 5 cm. The INEL counters also provide a minimum-bias trigger for the experiment. Based on GEANT simulations, they are sensitive to $91 \pm 3\%$ of the total inelastic cross section.

Reaction centrality is determined using a geometry-weighted average of SiMA and TMA multiplicities. Both the SiMA and TMA multiplicities are corrected for the distance of the actual interaction vertex from the nominal vertex at array center. GEANT simulations were used to correct for the possibility that neither the SiMA nor the TMA detectors will be hit by a particle for the most peripheral events.

Figure 1 shows the normalized SiMA and TMA averaged multiplicities. The observed falloff is unlike that of the corresponding Au + Au spectrum [9], where there is an extended "flat" region and a well-defined high multiplicity knee. The $d +$ Au spectrum instead reflects a smaller number of participants, making the measurements more sensitive to the underlying nucleon-nucleon collision multiplicity distribution. Also, the small particle multiplicities for $d +$ Au collisions result in a relatively large range in the fraction of particles detected for a given total number of particles emitted. The broad correlation band found in comparing SiMA and TMA multiplicities (Fig. 1 inset) illustrates the statistical scatter of the semi-independent multiplicity measurements. Reaction centralities are found by integrating the yield under the multiplicity curve. Limits for the 30%, 60%, and 80% centrality cuts are indicated by the vertical lines.

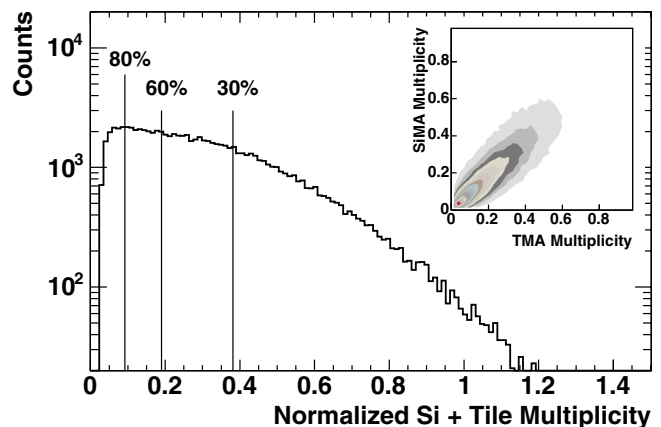Figure 2 shows the resulting charged-particle pseudorapidity-density plots for minimum-bias events

FIG. 1 (color online). SiMA and TMA averaged multiplicity distribution normalized to the 1% centrality level. Lines show efficiency corrected limits for indicated centralities. The inset shows the correlation between the SiMA and TMA multiplicities.
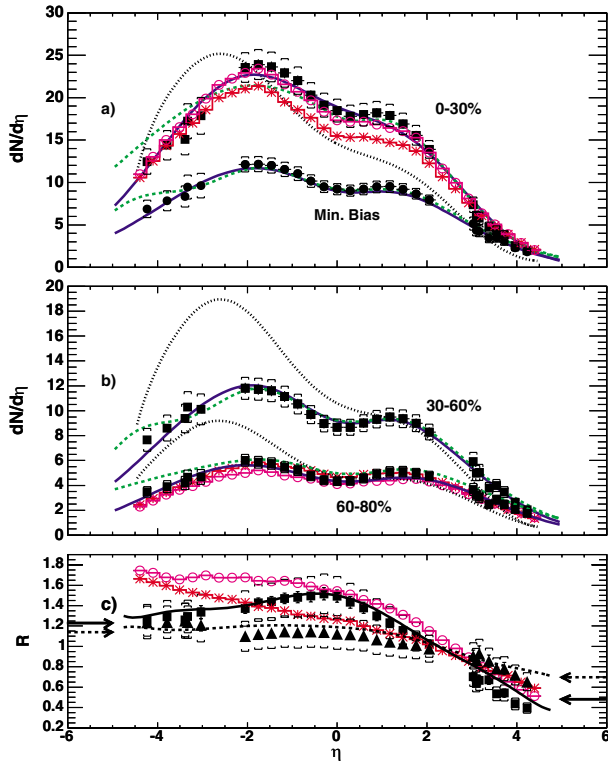
FIG. 2 (color online).   (a),(b) Charged-particle pseudorapidity
densities for indicated centrality ranges. (c) Multiplicity ratios
R^{0-30} (squares) and R^{30-60} (triangles), as discussed in the text.
Statistical uncertainties are indicated by vertical lines or are
smaller than the symbols. Detached horizontal brackets indicate
the total (statistical and systematic) uncertainties. The solid,
dashed, and dotted curves in (a) and (b) are the results of the
HIJING, AMPT, and Saturation models, respectively. The curves
in (c) show the HIJING results for R^{0-30} (solid line) and R^{30-60}
(dashed line), with the arrows indicating the values expected for
Au- and d-participant, only, scaling. In all panels, the connected
open circles (asterisks) correspond to unrestricted HIJING calcu-
lations with centrality classes based on multiplicity (impact
parameter), as discussed in the text.

and 0%–30%, 30%–60%, and 60%–80% centrality
classes. The SiMA and TMA results have been averaged.
Overall statistical uncertainties are indicated or are smaller
than the data points. Systematic uncertainties, denoted
by the horizontal brackets and estimated as 8% for the
averaged SiMA and TMA results and 12% for the BBC
values, are determined by exploring the variation of the
deduced pseudorapidity densities to reasonable changes in
the energy calibrations and background subtraction. Our
minimum-bias data agree within systematic uncertainties
with recently reported results [25].

Three model calculations are compared to the data. The
solid curves show the predictions of HIJING [12], a Monte
Carlo model that includes both soft and hard, perturbative
QCD-based scattering effects. The dashed curves show the
predictions of a multiphase transport (AMPT) model [13–
15] which includes both initial partonic and final hadronic

interactions. For comparison with experiment, both the
HIJING and AMPT model results have been filtered through
a GEANT [24] simulation of the BRAHMS experimental
response. Centrality is based on the fraction of events with
the highest particle multiplicity within the pseudorapidity
range of the SiMA and TMA arrays. Both models repro-
duce the experimental results at midrapidity and at positive
rapidities approaching the deuteron-fragmentation region.
At negative rapidity (Au-fragmentation region) the two
models start to diverge and here HIJING appears to be in
slightly better agreement with our results.

The dotted curves in Fig. 2 show the expectations of the
saturation model [5] which accounts for the high-density
QCD effects that are expected to limit the number of
partons in the entrance channel. In this case the centrality
dependence was based on the published curves of charged-
particle pseudorapidity densities for different centrality
ranges given in Ref. [5]. The model appears to be unsuc-
cessful in reproducing either the centrality or pseudorapid-
ity dependence of the present results.

The number of participant N_{part} scaled ratios of
central-to-peripheral $[R^{0-30} = (0.35 \pm 0.03)\{[dN^{0\%-30\%}/d\eta]/[dN^{60\%-80\%}/d\eta]\}]$ and midcentral-to-
peripheral $[R^{30-60} = (0.56 \pm 0.04)\{[dN^{30\%-60\%}/d\eta]/[dN^{60\%-80\%}/d\eta]\}]$ charged-particle densities are shown
in Fig. 2(c) along with the corresponding HIJING ratios
(curves). Here we take $\langle N_{part} \rangle = 13.6 \pm 0.3$, 8.5 ± 0.3,
and 4.7 ± 0.3 for the 0%–30%, 30%–60%, and 60%–
80% centrality ranges, respectively. The systematic un-
certainties for the ratios include the participant scaling
uncertainty and a 5% uncertainty for the experimental
pseudorapidity-density ratios. The participant ratios
appropriate for Au(left arrows)- and d(right arrows)-par-
ticipant-only scaling are shown in Fig. 2(c) for R^{0-30} (solid
line) and R^{30-60} (dashed line), respectively. The HIJING
model reproduces well the experimental ratios, as shown
in Fig. 2(c). In this regard, it can be noted that the mid-
rapidity pseudorapidity densities obtained in a stand-alone
HIJING calculation scale roughly as the number of Au
participants.

We use HIJING to explore the potential bias introduced by
the limited acceptance of the MA (SiMA and TMA) on the
deduced pseudorapidity distributions and R values. The
connected open circles in Fig. 2 show the results for the
0%–30% [panel (a)] and 60%–80% [panel (b)] centrality
classes of an unrestricted HIJING calculation where the
centrality is based on all charged particles emitted in the
reaction, and not just those that satisfy the experimental
acceptance. The greatest effect on the pseudorapidity dis-
tributions is found for the 60%–80% centrality cut and
amounts to as much as an 18% enhancement in the mea-
sured $dN/d\eta$ values in the Au-fragmentation region. The
corresponding R^{0-30} curve no longer shows evidence of the
midrapidity maximum observed for the experimental
results.

In lighter systems, the events selected in a given range of multiplicity-based centrality are not all the same as would be selected if it were possible to base centrality on the impact parameter. This is shown in Fig. 2 where the connected asterisks indicate the HIJING model $dN_{ch}/d\eta$ distributions for 0%–30% [panel (a)] and 60%–80% [panel (b)] centrality classes based on impact parameter, and the corresponding R^{0-30} ratio [panel (c)]. Here the R^{0-30} curve shows a steady rise from the d- to Au-fragmentation sides, illustrating that the centrality selection does affect the deduced $1/N_{part} \times dN_{ch}/d\eta$ values.

The $d + $Au system was previously studied by the NA35 experiment at $\sqrt{s_{NN}} = 19.4$ GeV [20] where data were obtained for both negative hadrons h^- and for the net baryons as measured by the difference of proton and anti-proton yields ($p - \bar{p}$). Pseudorapidity distributions were found corresponding to the most central 43% of the total inelastic cross section, with both deuteron nucleons acting as participants. For comparison with the present results, the total charged-particle densities are determined for the lower energy data taking $dN_{ch}/d\eta = 2 \times dN(h^-)/d\eta + dN(p - \bar{p})/d\eta$. The pseudorapidity densities are deduced from quoted rapidity distributions by first shifting to the center-of-mass system and then assuming the π^- mass for h^- and the observed mean-p_t values for the h^- and $p - \bar{p}$ distributions. At the higher energy of the current measurement, HIJING model simulations indicate that the criteria that both deuteron nucleons act as participants is well satisfied for the 0%–30% centrality range. In this case it is interesting to see if the limiting fragmentation behavior previously observed in Au + Au yields at $\sqrt{s_{NN}} = 130$ and 200 GeV [9,10] is present in the $d + $Au system.

Figure 3(a) compares the $d + $Au pseudorapidity distributions in the nucleon-nucleon center-of-mass system, where the fixed-target NA35 results have been shifted by the center-of-mass rapidity. A factor of 2.2 increase is seen in the charged-particle density at midrapidity for the higher energy data. Using HIJING to determine N_{part}, $\{[\langle N_{part}^{d+Au}(19.4 \text{ GeV})\rangle]/[\langle N_{part}^{d+Au}(200 \text{ GeV})\rangle]\} \times [(dN^{200 \text{ GeV}}/d\eta)/(dN^{19.4 \text{ GeV}}/d\eta)] = 1.7$. Although the different methods of event selection for the two experiments might reduce this value, the data do not support simple participant scaling with energy. Figure 3(b) compares the data at the two energies in the frame of the Au fragment, with the NA35 results scaled up by the ratio of Au participants at the two energies. The two distributions have similar values approaching the Au rapidity, although it should be noted that counting the number of participants in the heavier fragmentation region of a very mass-asymmetric reaction is difficult because of multiple scatterings in the target spectator matter [20]. The solid curve shows the results for the 0%–30% central Au + Au distribution at $\sqrt{s_{NN}} = 200$ GeV [10], scaled by the ratio of $d +$ Au gold participants to the number of Au + Au participant pairs. The current measurements do not extend close

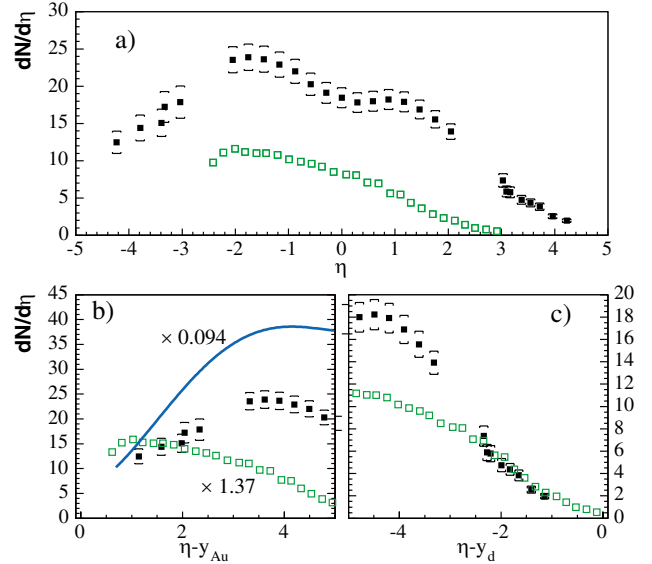FIG. 3 (color online). Comparison of central $\sqrt{s_{NN}} = 200$ GeV results (solid squares) with NA35 data (open squares) at $\sqrt{s_{NN}} = 19.4$ GeV in (a) the nucleon-nucleon center-of-mass system, (b) the Au rest frame, and (c) the deuteron rest frame. The solid curve is based on data for Au + Au 0%–30% central events at $\sqrt{s_{NN}} = 200$ GeV [10]. N_{part} scaling is applied as indicated in panel (b).

enough to the beam rapidities to assess limiting fragmentation scaling on the Au-fragmentation side. Figure 3(c) compares the two $d + $Au distributions in the deuteron frame. With the given centrality selections, $N_{part}(d) \approx 2$ at both energies and so no participant scaling is done for the comparison. The two distributions are found to overlap from roughly one to two units of pseudorapidity below beam rapidity, suggesting a limiting fragmentation behavior over at least this range.

Pseudorapidity densities of charged particles for the $d + $Au reaction at $\sqrt{s_{NN}} = 200$ GeV are presented for different centrality ranges. The ratio of particle densities for central and peripheral events is found to agree well with participant scaling in terms of the respective fragments away from midrapidity. Overall, model calculations based on both soft physics and perturbative QCD (HIJING, AMPT) lead to excellent agreement with the experimental results. Calculations based on the saturation picture using scale parameters set by previous experimental data fail to reproduce the measurements and lead to a pseudorapidity dependence very different from that observed with the current data. Comparison with lower energy $d + $Au data suggests a limiting fragmentationlike behavior near the rapidity of the deuteron fragment.

———

[1] L. V. Gribov, E. M. Levin, and M. G. Ryskin, Phys. Rep. **100**, 1 (1983).

[2] K. J. Eskola, K. Kajantie, and K. Tuominen, Phys. Lett. B **497**, 39 (2001).

[3] D. Kharzeev and E. Levin, Phys. Lett. B **523**, 79 (2001).

[4] D. Kharzeev and M. Nardi, Phys. Lett. B **507**, 121 (2001).

[5] D. Kharzeev, E. Levin, and M. Nardi, Nucl. Phys. **A730**, 448 (2004). An erratum to this reference discusses the sensitivity of the calculation to the assumed number of participants and presents a calculation in excellent agreement with our results [**A743**, 329 (2004)].

[6] B. B. Back *et al.*, Phys. Rev. Lett. **85**, 3100 (2000).

[7] C. Adler *et al.*, Phys. Rev. Lett. **87**, 112303 (2001).

[8] K. Adcox *et al.*, Phys. Rev. Lett. **86**, 3500 (2001).

[9] I. G. Bearden *et al.*, Phys. Lett. B **523**, 227 (2001).

[10] I. G. Bearden *et al.*, Phys. Rev. Lett. **88**, 202301 (2002).

[11] B. B. Back *et al.*, Phys. Rev. Lett. **88**, 022302 (2002).

[12] X. N. Wang and M. Gyulassy, Phys. Rev. D **44**, 3501 (1991); code HIJING 1.383.

[13] Bin Zhang, C. M. Ko, Bao-An Li, and Zi-wei Lin, Phys. Rev. C **61**, 067901 (2000).

[14] Zi-wei Lin, Subrata Pal, C. M. Ko, Bao-An Li, and Bin Zhang, Phys. Rev. C **64**, 011902R (2001).

[15] Zi-wei Lin, Subrata Pal, C. M. Ko, Bao-An Li, and Bin Zhang, Nucl. Phys. **A698**, 375c (2002).

[16] B. B. Back *et al.*, Phys. Rev. Lett. **91**, 072302 (2003).

[17] S. S. Adler *et al.*, Phys. Rev. Lett. **91**, 072303 (2003).

[18] J. Adams *et al.*, Phys. Rev. Lett. **91**, 072304 (2003).

[19] I. Arsene *et al.*, Phys. Rev. Lett. **91**, 072305 (2003).

[20] T. Alber *et al.*, Eur. Phys. J. C **2**, 643 (1998).

[21] Y. K. Lee *et al.*, Nucl. Instrum. Methods Phys. Res., Sect. A **516**, 281 (2004).

[22] S. Bültmann *et al.*, Phys. Lett. B **579**, 245 (2004).

[23] M. Adamczyk *et al.*, Nucl. Instrum. Methods Phys. Res., Sect. A **499**, 437 (2003).

[24] GEANT 3.2.1, CERN program library.

[25] B. B. Back *et al.*, Phys. Rev. Lett. **93**, 082301 (2004).